TTPOINT: A Tensorized Point Cloud Network for Lightweight Action Recognition with Event Cameras

Hongwei Ren*

The Hong Kong University of Science and Technology (Guangzhou) Nansha,Guangzhou, China hren066@connet.hkust-gz.edu.cn

> Yulong Huang MICS Trust,

The Hong Kong University of Science and Technology (Guangzhou) Nansha,Guangzhou, China yulonghuang@hkust-gz.edu.cn Yue Zhou* MICS Trust,

The Hong Kong University of Science and Technology (Guangzhou) Nansha,Guangzhou, China yzhou833@connet.hkust-gz.edu.cn

> Renjing Xu MICS Trust,

The Hong Kong University of Science and Technology (Guangzhou) Nansha,Guangzhou, China renjingxu@ust.hk Haotian Fu MICS Trust,

The Hong Kong University of Science and Technology (Guangzhou) Nansha,Guangzhou, China hfu373@connet.hkust-gz.edu.cn

> Bojun Cheng[†] MICS Trust,

The Hong Kong University of Science and Technology (Guangzhou) Nansha,Guangzhou, China bocheng@ust.hk

ABSTRACT

Event cameras have gained popularity in computer vision due to their data sparsity, high dynamic range, and low latency. As a bioinspired sensor, event cameras generate sparse and asynchronous data, which is inherently incompatible with the traditional framebased method. Alternatively, the point-based method can avoid additional modality transformation and naturally adapt to the sparsity of events. Still, it typically cannot reach a comparable accuracy as the frame-based method. We propose a lightweight and generalized point cloud network called TTPOINT which achieves competitive results even compared to the state-of-the-art (SOTA) frame-based method in action recognition tasks while only using 1.5% of the computational resources. The model is adept at abstracting local and global geometry by hierarchy structure. By leveraging tensortrain compressed feature extractors, TTPOINT can be designed with minimal parameters and computational complexity. Additionally, we developed a straightforward downsampling algorithm to maintain the spatio-temporal feature. In the experiment, TTPOINT emerged as the SOTA method on three datasets while also attaining SOTA among point cloud methods on all five datasets. Moreover, by using the tensor-train decomposition method, the accuracy of the proposed TTPOINT is almost unaffected while compressing the parameter size by 55% in all five datasets.

CCS CONCEPTS

• Computing methodologies → Computer vision tasks.

Permission to make digital or hard copies of all or part of this work for personal or classroom use is granted without fee provided that copies are not made or distributed for profit or commercial advantage and that copies bear this notice and the full citation on the first page. Copyrights for components of this work owned by others than the author(s) must be honored. Abstracting with credit is permitted. To copy otherwise, or republish, to post on servers or to redistribute to lists, requires prior specific permission and/or a fee. Request permissions from permissions@acm.org.

MM '23, October 29-November 3, 2023, Ottawa, ON, Canada

© 2023 Copyright held by the owner/author(s). Publication rights licensed to ACM. ACM ISBN 978-x-xxxx-xxxx-x/YY/MM...\$15.00 https://doi.org/10.1145/nnnnnnn.nnnnnn

KEYWORDS

tensorized network; event cameras; point cloud; action recognition

ACM Reference Format:

1 INTRODUCTION

Dynamic Vision Sensors (DVS) offer an attractive option for deploying lightweight networks that can perform real-time action recognition. Unlike conventional cameras that sample light intensity at fixed intervals, each DVS pixel independently responds to in situ gradient light intensity changes, signaling the corresponding point's movement in three-dimensional space [14]. This unique capability allows DVS cameras to capture sparse and asynchronous events that respond rapidly to changes in brightness. DVS cameras exhibit remarkable sensitivity to rapid light intensity changes, detecting log intensity in individual pixels and achieving event outputs typically in the order of a million events per second (Meps). In comparison, common cameras can only capture 60 frames per second, highlighting the unparalleled speed of DVS cameras [34]. Moreover, the unique operating principle of DVS cameras grants them superior power efficiency, low latency, less redundant information, and high dynamic range. As such, DVS cameras have found diverse applications in high-speed target tracking, simultaneous localization and mapping (SLAM) [25], and industrial automation.

Event stream contains information on the coordinates, time, and polarity of the event occurrence [22]. The temporal stream can distinguish fast behaviors within several microseconds [8]. Several studies have endeavored to extend and improve the problem of processing dynamic motion information from DVS. As shown in Figure 2 (a), the event stream data is segmented into small chunks, and the event for each time period will be mapped and accumulated into the image plane [9]. The grayscale on the plane will be stated

^{*}Both authors contributed equally to this research.

[†]Corresponding author.

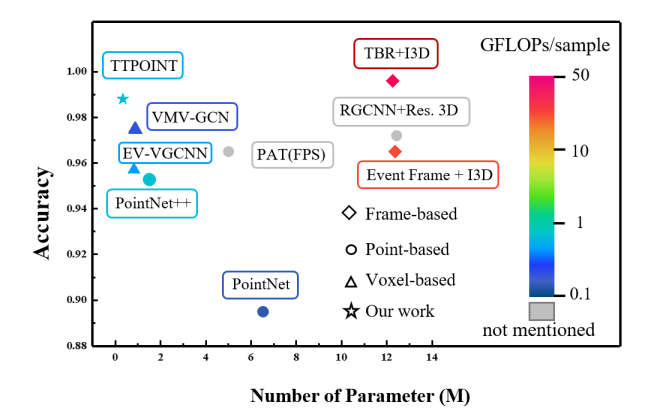


Figure 1: The gain in DVS128 Gesture of our work is visualized. TTPOINT achieves SOTA in the point-based method and maintains very high efficiency. The shapes utilized to illustrate the results correspond to different input data formats, with varying colors denoting FLOPs.

as the intensity of the event occurrence at that point. However, the framed-based method ignores the fine-grained temporal information within a frame, and the accumulated image gets blurred in fast-moving action scenarios. Moreover, this approach increases the data density and processing volume, diluting the sparse data benefits of an event-based camera. As a result, the frame-based method is unsuitable for scenarios with fast-moving actions and cannot be accomplished with limited computational resources.

In order to overcome the issues discussed above, alternative approaches, such as the point-based method have been proposed. This method is well-suited for analyzing DVS data as each event can be treated as a 3D point with coordinates (x, y, t), which can then be directly fed into the point cloud network, as shown in Figure 2 (b). By doing so, the data conversion process is greatly simplified, and the fine-grained temporal information is preserved [29]. However, it is worth noting that most existing efforts have been focused on optimizing the network structures, while relatively little attention has been paid to sampling points. As only a small fraction of all points (typically 0.1% to 1%) are sampled in the point cloud, it is important to ensure that they are sampled in a careful manner to avoid losing valuable information and to maintain high accuracy in action recognition. Since the point density of DVS events can vary over time, random sampling may not capture enough points in regions with low temporal point density, adversely affecting the capture of complete temporal information of actions.

Our primary goal is to democratize computer vision technology by making it accessible to a wider range of devices and applications. It is indeed accurate that conventional action recognition generally displays a negligible processor power consumption. However, with the advent of DVS technology, the power consumption of sensors has been drastically reduced by 90%-95%, rendering it much lower than that of conventional ANN processors. Consequently, decreasing the algorithm's power consumption has the potential to significantly reduce overall power consumption and

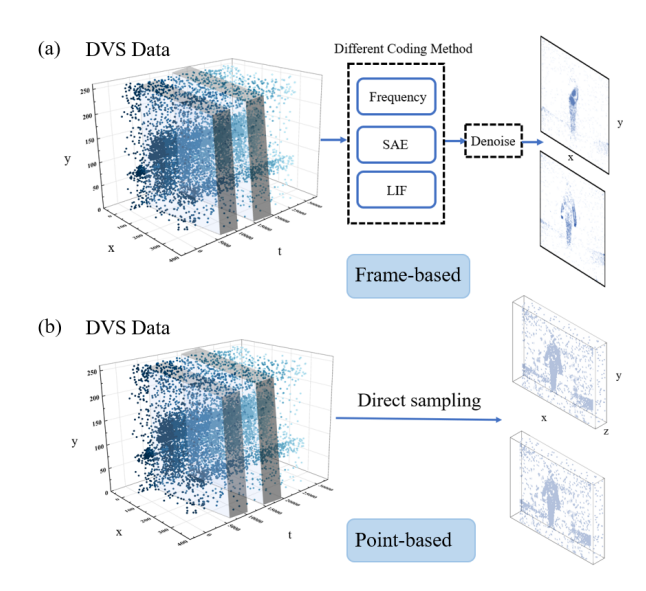


Figure 2: Two different methods of handling event streams, are (a) frame-based methods and (b) point-based methods. Frame-based methods compress a period of events into a grayscale image by SAE, LIF, etc.

enable the deployment of numerous battery-powered or resourceconstrained devices, such as mobile phones, drones, and IoT devices. To achieve this goal, we introduce a novel tensorized point cloud network, named TTPOINT, for event-based action recognition tasks, as shown in Figure 3. TTPOINT is characterized by its lightweight parameterization and computational demands, making it ideal for resource-constrained devices. It features a spatio-temporal prepossessing, a hierarchy structure composed of the tensor-train decomposition module, and a classifier. First, the event stream is divided into many sliding windows of fixed length. For each sliding window, we sample points from d subwindows to ensure the consistency of actions in time. Then, the sampled points are fed into a hierarchy structure to extract point cloud features. The hierarchy structure composes of a tensor-train decomposition module which makes up of residual local extractors and residual global extractors. Finally, the general classifier of Multi-Layer Perceptron (MLP) is used for action recognition. The main contributions of this work are:

- We propose a lightweight point-based network with a generalization ability to handle different-size event-based tasks.
- We affiliate the temporal information by subwindow sampling and obtain spatial features by the residual extractor, forming a spatio-temporal network structure.
- We utilize tensor-train decomposition to make the architecture lighter and more efficient with acceptable loss.

2 RELATED WORK

2.1 Frame-based Method

Frame-based methods have been extensively employed for event data processing. These methods convert events into a density map by integrating the number of events within a specific time interval, which can be visualized as a 2D image [13]. The resulting image can

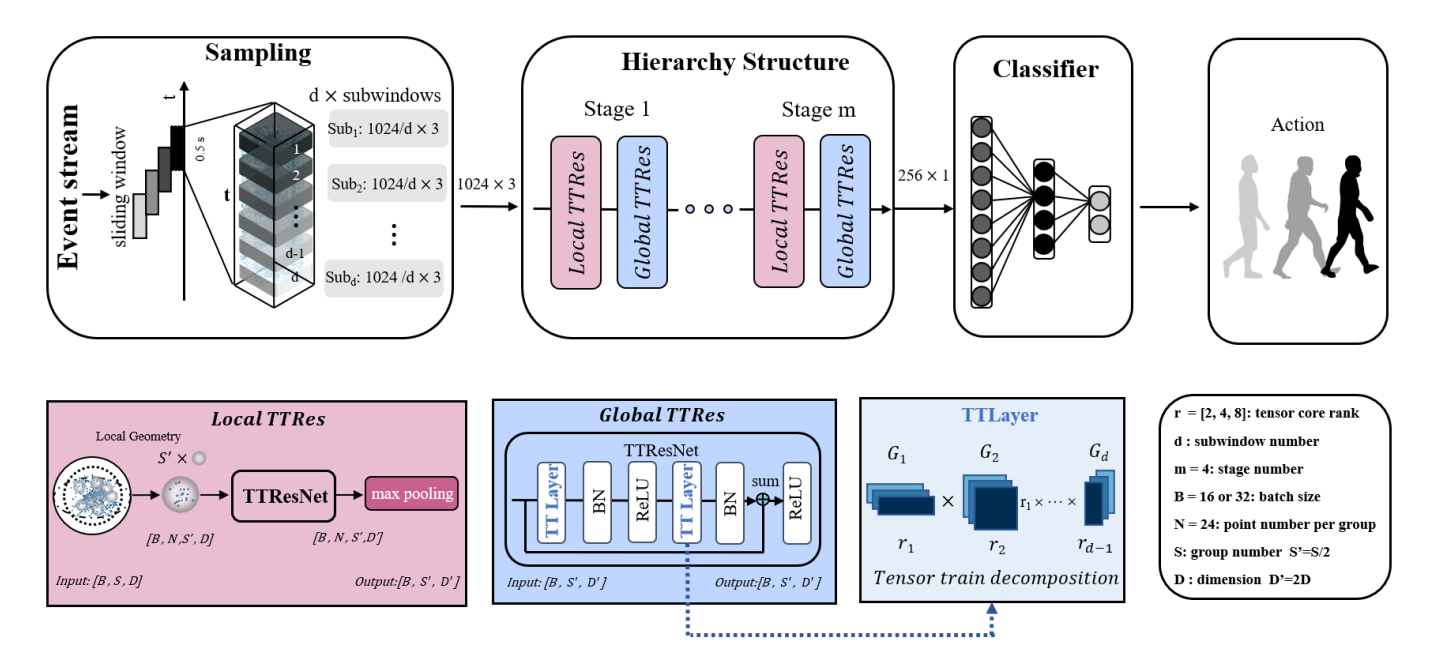


Figure 3: TTPOINT achieves action recognition by processing the event stream through several modules, namely sampling, hierarchy structure, and classifier. Specifically, LocalTTRes is in charge of extracting local geometric features, whereas GlobalTTRes serves to increase the dimensionality of the extracted features and abstract more high-level global features.

be directly fed into traditional feature extraction techniques such as Convolutional Neural Networks (CNNs) [1], RGCNNs [4], and Asynchronous Sparse Convolutional Networks [19], all of which have demonstrated high accuracy when using event input, as shown in Figure 1 for benchmarking purposes. However, these methods suffer from several limitations. For instance, the processed frame sizes are typically larger than those of the original event stream data, resulting in high computational costs and large model sizes. Furthermore, the aggression process introduces significant latency [9], which hinders the use of event cameras in real-time human-machine interaction applications.

2.2 Point-based Method

The emergence of PointNet [23] allows the point cloud to be processed directly as input. PointNet++ [24] adds the Set Abstraction (SA) module to determine the hierarchy architecture of global and local processing of the point cloud. Since the feature extractor of PointNet++ is still using simple MLP, more new methods have been added to improve the quality of point cloud methods. PointConv [31] uses deep convolution neural networks and deconvolution networks for point cloud processing. Transformer is improved to be more suitable for point cloud tasks and form the architecture of PointTransformer [35]. Recently, simple methods also achieve outstanding results. For example, PointMLP [17] leverages simple ResNet block and affine module and achieves SOTA results in point classification and segmentation tasks.

Applying the point-based method to the event stream requires processing the temporal information without loss of representation with x and y [27]. ST-EVNet [29] first achieved this and applied PointNet++ to complete the task of gesture recognition. PAT [33]

improved the model and achieved better performance in DVS128 Gesture by combining the self-attention mechanism and Gumbel subset sampling. However, these methods rely on random sampling, which fails to capture enough points in low temporal point density regions. Moreover, their models are not optimized for size and computational efficiency and cannot meet the demands of edge devices based on ARM-cortex-M [32]. Our approach builds upon the strengths of the point cloud, namely its sparse nature and low computational requirements. In contrast to prior methods, we propose a novel sampling algorithm that can capture events occurring at different temporal scales and varying movement speeds. To cater to real-time applications, we optimize the use of lightweight and sparse point-based methods and compress the model while maintaining high performance. Through a comprehensive evaluation of five action recognition datasets, we demonstrate the superiority of our approach over most frame-based methods in terms of accuracy, parameter size, and operational efficiency.

3 METHOD

Our approach builds on the strengths of the point-based method while enhancing the efficiency and effectiveness of the overall algorithm. We achieve this through an action-friendly sampling method. To achieve optimal lightweight design, we employ a hierarchical structure for the network, which is then further optimized and compressed to achieve a favorable balance between accuracy and network size.

3.1 Event stream

Event streams are time-series data that record spatial intensity changes of images in chronological order. A simple event can be

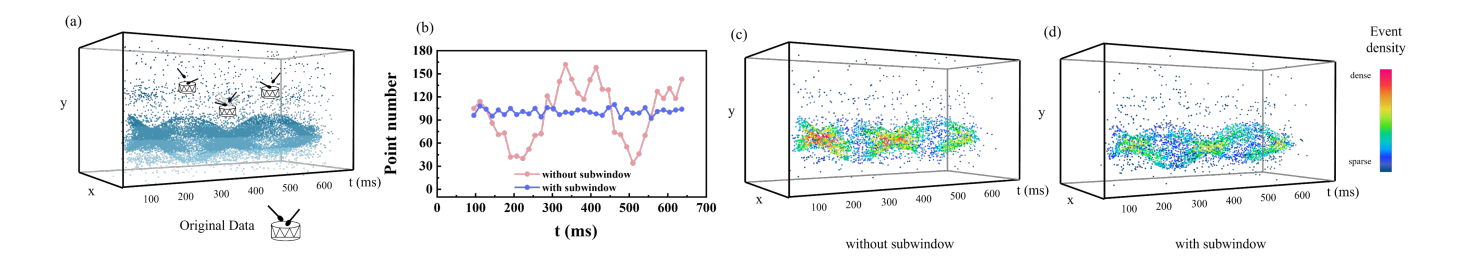


Figure 4: Visualization results on air drums action with and without subwindow. We visualize the dataset using different colors to denote the density of points, where red represents high density, and blue represents low density. The results are presented in various slices, with (a) showing the original point cloud of the air drums' action. We use statistical analysis to describe the change in point cloud density in the local range, with and without the subwindow, as shown in (b). We also present the point cloud after sampling without the subwindow in (c) and after sampling with the subwindow in (d).

expressed in $e_m = (x_m, y_m, t_m, p_m)$, where m stands for the index to identify the m-th element in the sequence. And the set of events in a single action recognition AR data can then be expressed as:

$$AR_{raw} = \{e_m = (x_m, y_m, t_m, p_m) \mid m = 1, ..., n\}$$
 (1)

To apply the point cloud method, four-dimensional e_m has to be simplified into a three-dimensional space-time event. A straight way to do this is to convert t_m into z_m :

$$AR_{point} = \{e_m = (x_m, y_m, z_m) \mid m = 1, 2, ..., n\}$$
 (2)

With $z_m = \frac{t_m - t_1}{t_n - t_1} \mid m \in (1, n)$, t_1 and t_n are the beginning and end timestamp of sliding windows, respectively. And x_m , y_m , z_m are normalized between [0, 1].

The sample is divided into sliding windows for two reasons. First, as shown in Table 1, the length of each sample in the action recognition dataset varies. Using the sliding window can normalize the sampling range within each sliding window. Second, the movement is repeated within a sample in most datasets, and the sliding window can isolate a single action from a set of repeated actions within the whole sample.

$$AR_{clip} = clip_i \{e_{k\longrightarrow l}\} \mid i \in (1, n_{win}) \mid t_l - t_k = L$$
 (3)

where L is the length of the sliding window, and n_{win} is the number of the sliding window. k and l are the timestamps of the starting and ending points of the i-th sliding window, respectively.

As previously stated, random sampling within the sliding window is straightforward and is widely used, but it has its limitations. The drawback is illustrated in Figure 4 with a 0.5 s slice window of air drum movement of the IBM DVS128 gesture dataset. As Figure 4 (b) shows, DVS yields a high density of events during rapid movement and a low density of events during slow movement. Therefore, the conventional random sampling method will get points from the moment with high movement speed, and slow movement is underrepresented. This can be seen clearly in 1024 randomly sampled points in Figure 4 (c).

To tackle this, we propose a further division strategy to ensure the capture of action events equally in the time domain. A

millisecond-level subwindow is introduced:

$$clip = \{sub_i \{e_{a \longrightarrow b}\} \mid i \in [0, n_{sub}] \mid t_b - t_a = L_{sub}\}$$
 (4)

where L_{sub} is the length of the subwindow, and n_{sub} is the number of the subwindow. So when events are sampled within a 0.5 s slice, the sampling point of each subwindow is the number of points (N) divided by n_{sub} . As such, the points are more equally sampled over time and guarantee even slow movement can be represented, as illustrated in Figure 4 (b), (d). In the next section, we will list the experimental results and compare the impact of different sampling points on performance.

3.2 Network

In this section, we provide a detailed exposition of the network architecture and present a formal mathematical representation of the model.

When we get a series of 3D data $clip_{sample}$ whose dimension is [1, 1024, 3] from the event stream through the above sampling method, we can input the data into the uncompressed model for point cloud feature extraction. We adopt the residual structure in the event processing field, which is proven to achieve excellent results in the point cloud field [17]. Next, we will introduce the design of the feature extractor for the uncompressed model.

$$\mathcal{P}_i = Max(LocalRes(S_{i-1})) \tag{5}$$

$$S_i = GlobalRes(\mathcal{P}_i) \tag{6}$$

$$F = S_m, \quad S_0 = clip_{sample}, where \quad i \in (1, m)$$
 (7)

where F is the extracted point cloud feature, which can be sent into the classifier to complete the task of action recognition. The uncompressed model has the ability to extract global and local features and has a hierarchy structure [24]. And the dimension of LocalRes input \in is [B, S, D], m is the number of stages for hierarchy structure, Max is the operation of max-pooling, $\mathcal P$ is the output of LocalRes, and the dimension of GlobalRes input \in [B, S', D'], as illustrated in Figure 3. B is the batch size, N is the point number of a group, D is the dimension of data, and S is the number of groups in overall point cloud data. From a macro perspective, LocalRes is mainly used to extract the local features of the spatial domain and

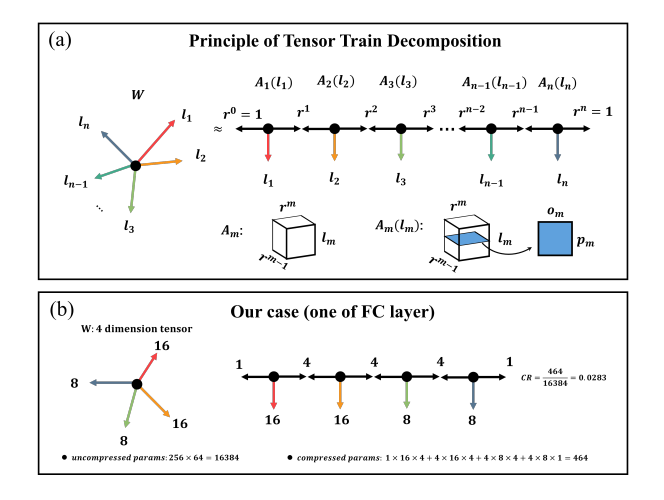


Figure 5: The tensor train decomposition of a *n*-dimensional tensor *W* model. Each black dot represents a tensor core, and the lines around the tensor core represent the dimensions.

operate the local through the farthest point sampling and grouping method. *GlobalRes* mainly synthesizes the extracted local features and establishes the global relationship.

Stacking Residual blocks can improve the learning ability of the model, but for sparse event-based data, how to trade off the parameters, computation, and accuracy is a key issue. Compared with the frame-based method, the advantage of point cloud processing is that the amount of data required is small, and the characteristics of events can be utilized. If the point cloud network with similar parameters and computation of frame-based method, it will lose the superiority of using the point cloud to process events. The Residual block can be written as a formula:

$$M(x) = BN(MLP(x)) \tag{8}$$

$$Res = \mathcal{F}(x + M(\mathcal{F}(M(x)))) \tag{9}$$

where \mathcal{F} is a nonlinear activation function ReLu, x is the input features, BN is batch normalization, and MLP is the muti-layer perception module.

3.3 Tensor train decomposition

To achieve the necessary levels of lightweight to surpass even the most advanced voxel-based methods and enable real-time processing on resource-constrained devices, tensor decomposition techniques hold great promise[21]. Among these, the tensor-train decomposition (TTD) framework has several notable advantages over more conventional approaches such as Canonical Polyadic (CP) decomposition and Tucker decomposition.

Firstly, TTD is highly efficient at handling high-dimensional tensors, reducing storage complexity from $O(n^d)$ to $O(d \cdot n \cdot r^2)$ and computational complexity from $O(n^{2d})$ to $O(d \cdot n \cdot r^3)$ (where n is the dimension of the tensor, d is the order of the tensor, and r is the rank size). Secondly, TTD requires only setting the rank size to balance accuracy and model size, whereas CP decomposition requires specifying the shape of each tensor and introducing additional hyperparameters. Thirdly, the size of each decomposed tensor

kernel is uniform in TTD, while Tucker decomposition features a super-large core tensor, posing a challenge for edge computation. Moreover, the feature extractor in our proposed TTPOINT network is implemented using multilayer perceptrons (MLPs), which is a perfect match for the TTD framework. Our experiments confirm the superior performance of TTPOINT leveraging TTD in event-based action recognition tasks.

We use the tensor-train decomposition method to compress the Res module, which will be described in detail below. A n-dimensional tensor $W \in R^{l_1 \times l_2 \times ... \times l_n}$ can be approximated by a number of tensor cores $\mathcal{A}_m \in R^{r_{m-1} \times l_m \times r_m} (m \in [1, n])$, where $W(l_1, l_2, ..., l_n)$ is an element specified by the indices $l_1, l_2, ..., l_n$, expressed as follows:

$$W(l_1, l_2, ..., l_n) = \mathcal{A}_1(l_1)\mathcal{A}_2(l_2)...\mathcal{A}(l_n)$$
(10)

 $\mathcal{A}_m(l_m) \in R^{r_{m-1} \times r_m}$ is a matrix slice from the 3-dimensional tensor \mathcal{A}_m and r_m is the rank of \mathcal{A}_m . For each integer l_m , it can be further decomposed as $l_m = o_m \times p_m$, where o and p represent the width of the two-layer neural network. Considering the example illustrated in Figure 5 (b) with l=16384, the original model has been reshaped into a four-dimensional tensor with the weight, denoted as l_m =[16,16,8,8], meaning $16\times16\times8\times8$ =16384. Likewise, the model with o=256 and p=64 also been reshaped in o_m =[4,4,4,4], and p_m =[4,4,2,2]. As a result, each tensor core \mathcal{A}_m can be transformed and reformed into $\mathcal{A}_m^* \in R^{r_{m-1} \times r_m \times o_m \times p_m}$. The double-index trick, as such is the core function to decompose the fully-connected computation in MLP cells.

$$W((o_1, p_1), (o_2, p_2), ..., (o_n, p_n))$$

$$= \mathcal{A}_1^*(o_1, p_1)\mathcal{A}_2^*(o_2, p_2)...\mathcal{A}_n^*(o_n, p_n)$$
(11)

The whole compression process of \mathcal{W} is illustrated in Figure 5 (a), and (b) represents a specific scenario with unique data to facilitate comprehension. If they are in CNN, they represent the height and width of the image, and if they are in the point cloud processing, they represent the input and output dimension values. In general, the large-scale matrix-vector multiplication is the most expensive computation in the MLP cell, generically denoted as:

$$\mathcal{Y} = \mathcal{W}\mathcal{X} + \mathcal{B} \tag{12}$$

To approximates WX with much fewer parameters, the weight matrix W is reshaped into a tensor $W \in R^{(o_1 \times o_2 \times \ldots \times o_n) \times (p_1 \times p_2 \times \ldots \times p_n)}$. Similarly, X and \mathcal{B} can be reshaped into n-dimentional tensors $X \in R^{l_1 \times l_2 \times \ldots \times l_n}$ and $\mathcal{B} \in R^{l_1 \times l_2 \times \ldots \times l_n}$. As a result, the output y can also become a n-dimentional tensor $\mathcal{Y} \in R^{l_1 \times l_2 \times \ldots \times l_n}$. Therefore, the matrix-vector multiplication in MLP cells can be reformulated as follows:

$$\mathcal{Y}(l_1, l_2, ..., l_n) = \sum_{m} ... \sum_{n} [\mathcal{R}_1^*(o_1, p_1) \\ \mathcal{R}_2^*(o_2, p_2) ... \mathcal{R}_n^*(o_n, p_n) \mathcal{X}] + \mathcal{B}(l_1, l_2, ..., l_n)$$
(13)

Due to the tensor decomposition strategy, the computational complexity in the tensor-compressed MLP decreases a lot. For the basic uncompressed model mentioned above, after compression, the model size is compressed by 55% to merely 0.334 M, and the number of floating-point operations is reduced to 0.587 GFLOPs by 46%. In TTPOINT, we replace the MLP in Res block with TTlayer which is compressed MLP by the formula:

$$\mathcal{T}(x) = BN(TTlayer(x))$$
 (14)

$$TTRes = \mathcal{F}(x + \mathcal{T}(\mathcal{F}(\mathcal{T}(x)))) \tag{15}$$

$$\mathcal{P}_i = Max(LocalTTRes(ST_{i-1})) \tag{16}$$

$$ST_i = GlobalTTRes(\mathcal{P}_i)$$
 (17)

$$TTPOINT = ST_m$$
, $ST_0 = clip_{sample}$, where $i \in (1, m)$ (18)

where the rank of TTlayer will provide in the next section. A lite point cloud network with tensor train decomposition is set up.

4 EXPERIMENT

In this section, we train and test the performance of the proposed model on the server platform. The experiment includes the accuracy performance of the model on the datasets, the size of model parameters, and the number of floating-point operations (FLOPS). The specific parameters of our platform are CPU: AMD 7950x, GPU: RTX 4090, and Memory: 32GB.

4.1 Datasets

We evaluate TTPOINT on five popular action recognition datasets. The resolution, total classes, and other information of each dataset are shown in Table 1.

Daily DVS dataset [15] contains 1440 recordings of 15 subjects performing 12 different common daily actions, such as standing up, walking, and carrying boxes. Each subject performed each action under the same conditions, and the recordings are all within 6 seconds.

DVS128 Gesture dataset [1] is 11 classes of gestures collected by IBM in the actual environment with the iniLabs DAVIS128 camera. The sample resolution of this dataset is 128×128. That is, the coordinate value range of x and y is [1, 128]. The dataset includes 1342 examples, divided into 122 experiments that collected 29 subjects under different lighting conditions.

DVS Action dataset [20] is 10 classes of action collected with DAVIS346 camera. The sample resolution of this dataset is 346×260. The dataset was recorded in an empty office, and 15 subjects performed 10 different actions. The record file is named after each action, such as crossing arms, getting up, kicking, picking up, jumping, sitting down, throwing, turning, walking, and waving.

HMDB51-DVS and UCF101-DVS datasets [4] are converted from the dataset collected by traditional cameras, and the conversion mode uses DAVIS240. UCF101 contains a collection of 13,320 videos demonstrating 101 unique human actions, whereas HMDB51 consists of 6,766 videos depicting 51 categories of human actions. The sample resolution of these datasets is 320×240.

4.2 Implement Details

4.2.1 Pre-processing. The time set for sliding windows is 0.5 s, 1 s, or 1.5 s. In the DVS128 Gesture dataset and DVS Action dataset, the coincidence area of adjacent windows is set as 0.25 s. In other datasets, this is set to 0.5 s. Since there are many noises in the DVS Action dataset during the actual recording, we use the denoising method to reduce the probability of sampling noise points, and this dataset has no labels. After we are statist and visualize the files, we find that almost all actions occur after half of the total dataset, so when we build the dataset, the sampling start point starts from half of the total timestamps. Compared with the manual annotation

method [29], our method is slightly rough but still achieves better results on the DVS Action dataset.

4.2.2 Network Structure. The rank of tensor train decomposition affects the size of the compressed model and its performance on the dataset, so it is important to select an appropriate rank [18]. The rank of TTPOINT is 8, and the maximum compression ratio can reach 14. Additionally, we set this value to 4 in the ablation study for intensive compression, and the maximum compression ratio can reach 53, and the parameter quantity reduces by 0.03 M. We made statistics on the width of MLP in the model. Following the change of network parameters, the width is distributed in the set [1024, 512, 256, 128, 64, 32, 16]. So we set to rank as follows according to experience, 1024: [8, 8, 4, 4], 512: [8, 4, 4, 4], 256: [4, 4, 4], 128: [4, 4, 4, 2], 64: [4, 4, 2, 2], 32: [4, 2, 2], 16: [2, 2, 2, 2]. TTPOINT is divided into three modules: preprocess module, feature extractor, and classifier. Consult [17], we used four stages of the TTResidual block. The number of k-nearest neighbors for local feature extraction is 24.

4.2.3 Training Hyperparameter. Our training model uses the following hyperparameters, Batch Size: 16 or 32, Number of Points: 1024, Optimizer: momentum, Initial Learning Rate: 0.1, Scheduler: cosine, Max Epochs: 350.

4.3 Results of Action Recognition

4.3.1 Daily DVS. TTPOINT outperformed all methods and achieved an accuracy of 99.1% on this dataset, as shown in Table 2. However, despite using nearly 80 times more parameters, the frame-based method still yielded poor accuracy. We visualize the event stream in this dataset, which featured high recording quality, minimal noise, and clear actions. By using the point cloud sampling method, we could accurately capture the motion characteristics of actions. Initially, we employed a sliding window of 0.5 s, but this only approximately resulted in an accuracy of 85%. After adjusting it to 1.5 s, TTPOINT achieved remarkable accuracy of 99.1%, clearly demonstrating its superiority over other methods.

4.3.2 DVS128 Gesture. Table 3 shows the performance and network size of DVS 128 Gesture. The highest accuracy achieved is 99.6% [13]. However, this approach is frame-based and requires a large amount of memory for storage and calculation, which is about 50 times larger than our model. With model compression, TTPOINT has a parameter size of only 0.334 M and a total number of floating-point operations of 0.587 GFLOPs, while still achieving an accuracy of 98.8% on the DVS128 Gesture dataset. The parameter quantity of our method is greatly reduced, but the FLOPs are not reduced as much, possibly due to more operations on the original basis in the tensor-train method. It's also worth noting that TTPOINT achieved an accuracy of 97.8% on the sliding window testset. By utilizing a voting method on individual event streams, the classification result with the highest number of votes shows remarkable accuracy across 240 test sequences.

4.3.3 DVS Action. Table 4 illustrates the performance of the TT-POINT for DVS Action. TTPOINT achieves an accuracy rate of 92.7% on the DVS Action dataset. However, it can be seen from the number of training and test samples of the dataset that DVS Action is smaller than others. The knowledge learned from the

Dataset	Classes	Sensor	Resolution	Avg.length(s)	Train Samples	Test Samples	Sliding window	Overlap
Daily DVS [15]	12	DAVIS128	128x128	6	2924	731	1.5s	0.5s
DVS128 Gesture [1]	10/11	DAVIS128	128x128	6.52	26796	6959	0.5s	0.25s
DVS Action [20]	10	DAVIS346	346x260	5	912	116	0.5s	0.25s
HMDB51-DVS [4]	51	DAVIS240	320x240	8	24463	6116	0.5s	0.5s
UCF101-DVS [4]	101	DAVIS240	320x240	6.6	119214	29803	0.5s	0.5s

Table 1: Information of different action recognition datasets with event camera.

Name	Param.(x10 ⁶)	GFLOPs	Acc
I3D[5]	49.19	59.28	0.962
TANet[16]	24.8	65.94	0.965
VMV-GCN [32]	0.84	0.33	0.941
TimeSformer [3]	121.27	379.7	0.906
Motion-based SNN [15]	-	-	0.903
TTPOINT	0.335	0.587	0.991

Table 2: Model's accuracy and complexity on Daily DVS.

Method	Param.(x10 ⁶)	GFLOPs	Acc
TBR+I3D [13]	12.25	38.82	0.996
Event Frames + I3D [4]	12.37	30.11	0.965
EV-VGCNN [7]	0.82	0.46	0.957
RG-CNN [20]	19.46	0.79	0.961
PointNet++ [29]	1.48	0.872	0.953
VMV-GCN [32]	0.86	0.33	0.975
TTPOINT	0.334	0.587	0.988

Table 3: Model's accuracy and complexity on DVS128 Gesture.

Method	Param.(x10 ⁶)	GFLOPs	Num.	Acc
Deep SNN [10]	-	-	-	0.712
Motion-based SNN [15]	-	-	-	0.781
PointNet [23]	3.46	0.450	512	0.751
ST-EVNet [30]	1.6	-	1024	0.887
TTPOINT	0.334	0.587	1024	0.927

Table 4: Model's accuracy and complexity on DVS Action.

Method	Param.(x10 ⁶)	GFLOPs	Acc
C3D [28]	78.41	39.69	0.417
I3D [5]	12.37	30.11	0.466
ResNet-34 [12]	63.70	11.64	0.438
ResNext-50 [11]	26.05	6.46	0.394
ST-ResNet-18 [26]	-	-	0.215
RG-CNN [4]	3.86	12.39	0.515
TTPOINT	0.345	0.587	0.569

Table 5: Model's accuracy and complexity on HMDB51-DVS.

large model may be overfitted, and the representation ability of the compressed model is weakened to a certain extent so that it can perform better on this small dataset. We use the same model architecture on the five datasets and do not design targets for each dataset. This means that we may get better results if we adjust the architecture for different datasets.

4.3.4 HMDB51-DVS. The first three datasets are a few categories of action recognition datasets, so the HMDB51-DVS dataset is used

Name	Param.(x10 ⁶)	GFLOPs	Acc
C3D [28]	78.41	39.69	0.472
ResNext-50.3D [11]	26.05	6.46	0.602
I3D [5]	12.37	30.11	0.635
RG-CNN [4]	6.95	12.46	0.632
ECSNet [6]	-	12.24	0.702
Event-LSTM [2]	21.4	-	0.776
TTPOINT	0.357	0.587	0.725

Table 6: Model's accuracy and complexity on UCF101-DVS.

to verify whether the proposed method can be generalized to large datasets. Compared with the DVS128 Gesture dataset, we found that other methods, which are frame-based or voxel-based must increase the parameters several times or even dozens of times in order to learn the knowledge of this dataset. We can discover from Table 5 that the TTPOINT with the same structure can achieve perfect results. It also can be seen from Table 5 that the number of parameters is not consistently compared with the DVS128 Gesture dataset's model only because the final classifier's output has changed from 10 to 51. Moreover, the TTPOINT can be expanded to accommodate such complicated tasks, and we project a further improvement of the accuracy by increasing the TTPOINT's size.

4.3.5 UCF101-DVS. To further validate the generalization and effectiveness of TTPOINT, we conducted tests on a larger dataset with 101 classification results. The performance of TTPONT is shown in Table 6, not surpassing Event-LSTM as the second-best model. After being divided into sliding windows, the trainset of UCF101-DVS reached as high as 1192014, which is a huge challenge for the model. We still haven't changed the model except for modifying the output of the classifier to 101 classes. TTPOINT achieved an accuracy of 72.5%, and we envision increasing model complexity, which may further improve the accuracy.

In summary, we used the same TTPOINT to conduct a comprehensive evaluation of small, medium and large datasets. We found that TTPOINT is a model with the ability to generalize and achieve very good results on data of different sizes without the need for a targeted design of the network structure.

4.4 Ablation Study

4.4.1 The time interval of subwindow. To evaluate the new pre-processing method, we apply four different pre-processing parameters and train the TTPOINT with both the DVS128 Gesture dataset and the DVS Action dataset. The results are summarized in Table 7. We uniformly sample subwindows on the millisecond timesteps axis based on the sliding windows to ensure that the points and actions sampled on the time axis are strongly correlated. The length

Subwinow(x10 ³ µs)	No subwindow	250	125	62.5
DVS128 Gesture [1]	0.970	0.973	0.978	0.975
Improve(%)	-	0.3	0.8	0.5
DVS Action [20]	0.875	0.906	0.927	0.911
Improve(%)	-	3.1	5.2	3.6

Table 7: The improvement of accuracy on different lengths of subwindow which is 6.25×10^4 , 1.25×10^5 , 2.5×10^5 and 5×10^5 timestamps.

Dataset	Uncompressed Model	TTPOINT	TTPOINT_tiny
Daliy DVS [15]	0.990	0.991	0.988
DVS Action [20]	0.911	0.927	0.885
DVS128 Gesture [1]	0.975	0.978	0.970
HMDB51-DVS [4]	0.590	0.569	0.545

Table 8: The effect of performance with tensor-train decomposition. When working with datasets that are small to medium-sized, compression may result in positive outcomes. However, when dealing with larger datasets, compression may be less beneficial and could even lead to negative effects.

of the subwindows is set to four different values. We train TTPOINT with four different pre-processing data from the DVS128 Gesture dataset and DVS Action, and one does not use the subwindows method and another three uses. After repeated experiments, the best performance of TTPOINT on the two datasets is obtained. It finds that the accuracy of the model using the subwindow method was nearly 0.8% higher with 0.978 and 0.970 in DVS128 Gesture, and the accuracy of the model using the subwindow method was near 5.2% higher with 0.927 and 0.875 in DVS Action. In addition, we find that the accuracy of the model decreases as the number of subwindows increases from 125 to 62.5. We infer this phenomenon occurs because too many subwindow sampling distracts the model from the point-dense region, resulting in a dilution of important information. So in different scenarios, the optimized subwindow number may be different which is up to the speeds of the movement.

4.4.2 The effect with compression. We conducted a comparison between the accuracy of uncompressed models, TTPOINT, and TTPOINT_tiny, which is mentioned in 4.2.2 with the rank of 4, across three datasets of different sizes, as shown in Table 8. Surprisingly, we found that the accuracy of the model improved on the DVS ACTION, Daily DVS, and DVS128 Gesture datasets, but there were more severe drop points in the HMDB51-DVS dataset. We must emphasize that the models are identical, except for the classifier, across the five different-sized datasets. We suspect that for small datasets, overfitting was prevalent, but the use of tensor train decomposition effectively reduced this phenomenon, as shown by the rising trend in the testset results. Conversely, for the HMDB51-DVS dataset, which is significantly larger than the others, we observed underfitting and a substantial loss in accuracy due to excessive compression. We proposed two potential solutions: increasing the rank size of tensor train decomposition or modifying the structure to make it more complex. Furthermore, it is important to note that overly aggressive compression can result in suboptimal model performance. This was demonstrated by TTPOINT_tiny, which showed a decrease in accuracy due to excessive compression.

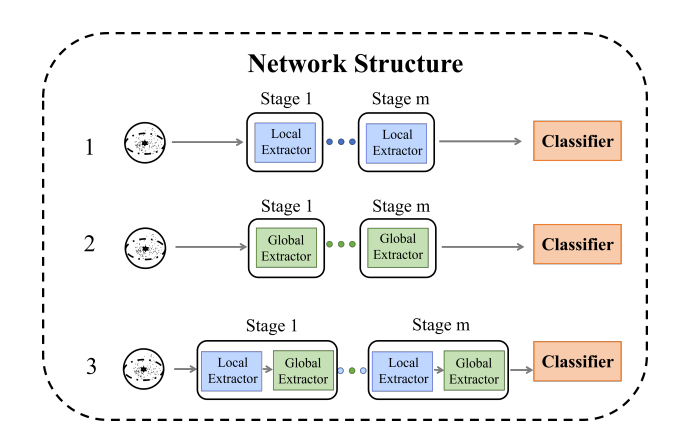


Figure 6: The ablation study on the local and global extractor. Method 1: only with local extractor block; Method 2: only with global extractor block; Method 3: apply both the local global extractor

Ultimately, the level of compression that should be applied depends on the desired balance between model accuracy and parameter quantity in practical applications.

4.4.3 The local and global extractor. To investigate the contribution of local and global feature extractors in the entire model, we conducted three comparative experiments on DVS128 Gesture as shown in Figure 6. The first experiment group, TTPOINT, lacked global feature extractors, the second group lacked local feature extractors, and the third group had both. Their respective accuracy on the sliding window testset was 96.19%, 90.2%, and 97.78%. These experimental results indicate that the local feature extractor is a crucial component of the model's performance, while the global feature extractor contributes to further improving the model's accuracy. TTPOINT's overall architecture without the local feature extractor is similar to PointNet, which results in poor performance due to the loss of local geometry information in the point cloud. Compared to other point-based methods, TTPOINT has a hierarchical structure similar to PointNet++'s Set Abstraction(SA). However, our model stands out thanks to its lightweight and efficient extractor design, offering not only ultra-high accuracy but also being sufficiently lightweight.

5 CONCLUSION

We propose a lightweight point cloud network named TTPOINT specifically for event camera action recognition, evaluate it on five mainstream corresponding datasets, and obtain excellent results. It performs well in accuracy and is suitable for low-latency applications with limited computational power.

In our future work, we will devote ourselves to the architecture development of the combination of point cloud processing network and spiking neural network (SNN) and can design a neuromorphic computing algorithm that is hardware and software friendly.

REFERENCES

 Arnon Amir, Brian Taba, David Berg, Timothy Melano, Jeffrey McKinstry, Carmelo Di Nolfo, Tapan Nayak, Alexander Andreopoulos, Guillaume Garreau,

- Marcela Mendoza, et al. 2017. A low power, fully event-based gesture recognition system. In *Proceedings of the IEEE conference on computer vision and pattern recognition*. 7243–7252.
- [2] Lakshmi Annamalai, Vignesh Ramanathan, and Chetan Singh Thakur. 2022. Event-LSTM: An unsupervised and asynchronous learning-based representation for event-based data. IEEE Robotics and Automation Letters 7, 2 (2022), 4678–4685.
- [3] Gedas Bertasius, Heng Wang, and Lorenzo Torresani. 2021. Is space-time attention all you need for video understanding?. In ICML, Vol. 2. 4.
- [4] Yin Bi, Aaron Chadha, Alhabib Abbas, Eirina Bourtsoulatze, and Yiannis Andreopoulos. 2020. Graph-based spatio-temporal feature learning for neuromorphic vision sensing. IEEE Transactions on Image Processing 29 (2020), 9084–9098.
- [5] Joao Carreira and Andrew Zisserman. 2017. Quo vadis, action recognition? a new model and the kinetics dataset. In proceedings of the IEEE Conference on Computer Vision and Pattern Recognition. 6299–6308.
- [6] Zhiwen Chen, Jinjian Wu, Junhui Hou, Leida Li, Weisheng Dong, and Guangming Shi. 2022. ECSNet: Spatio-Temporal Feature Learning for Event Camera. IEEE Transactions on Circuits and Systems for Video Technology (2022).
- [7] Yongjian Deng, Hao Chen, Huiying Chen, and Youfu Li. 2021. EV-VGCNN: A voxel graph CNN for event-based object classification. arXiv preprint arXiv:2106.00216 (2021).
- [8] Guillermo Gallego, Tobi Delbrück, Garrick Orchard, Chiara Bartolozzi, Brian Taba, Andrea Censi, Stefan Leutenegger, Andrew J Davison, Jörg Conradt, Kostas Daniilidis, et al. 2020. Event-based vision: A survey. IEEE transactions on pattern analysis and machine intelligence 44, 1 (2020), 154–180.
- [9] Daniel Gehrig, Antonio Loquercio, Konstantinos G Derpanis, and Davide Scaramuzza. 2019. End-to-end learning of representations for asynchronous eventbased data. In Proceedings of the IEEE/CVF International Conference on Computer Vision. 5633–5643.
- [10] Pengjie Gu, Rong Xiao, Gang Pan, and Huajin Tang. 2019. STCA: Spatio-temporal credit assignment with delayed feedback in deep spiking neural networks.. In IJCAI. 1366–1372.
- [11] Kensho Hara, Hirokatsu Kataoka, and Yutaka Satoh. 2018. Can spatiotemporal 3d cnns retrace the history of 2d cnns and imagenet?. In Proceedings of the IEEE conference on Computer Vision and Pattern Recognition. 6546–6555.
- [12] Kaiming He, Xiangyu Zhang, Shaoqing Ren, and Jian Sun. 2016. Deep residual learning for image recognition. In Proceedings of the IEEE conference on computer vision and pattern recognition. 770–778.
- [13] Simone Undri Innocenti, Federico Becattini, Federico Pernici, and Alberto Del Bimbo. 2021. Temporal binary representation for event-based action recognition. In 2020 25th International Conference on Pattern Recognition (ICPR). IEEE, 10426–10432.
- [14] Patrick Lichtsteiner, Christoph Posch, and Tobi Delbruck. 2008. A 128 \times 128 120 dB 15 μ s latency asynchronous temporal contrast vision sensor. *IEEE journal of solid-state circuits* 43, 2 (2008), 566–576.
- [15] Qianhui Liu, Dong Xing, Huajin Tang, De Ma, and Gang Pan. 2021. Event-based Action Recognition Using Motion Information and Spiking Neural Networks.. In IJCAI. 1743–1749.
- [16] Zhaoyang Liu, Limin Wang, Wayne Wu, Chen Qian, and Tong Lu. 2021. Tam: Temporal adaptive module for video recognition. In Proceedings of the IEEE/CVF international conference on computer vision. 13708–13718.
- [17] Xu Ma, Can Qin, Haoxuan You, Haoxi Ran, and Yun Fu. 2022. Rethinking network design and local geometry in point cloud: A simple residual mlp framework. arXiv preprint arXiv:2202.07123 (2022).
- [18] Changhai Man, Cheng Chang, Chenchen Ding, Ao Shen, Hongwei Ren, Ziyi Guan, Yuan Cheng, Shaobo Luo, Rumin Zhang, Ngai Wong, et al. 2023. RankSearch: An

- Automatic Rank Search Towards Optimal Tensor Compression for Video LSTM Networks on Edge. In 2023 Design, Automation & Test in Europe Conference & Exhibition (DATE). IEEE, 1–2.
- [19] Nico Messikommer, Daniel Gehrig, Antonio Loquercio, and Davide Scaramuzza. 2020. Event-based asynchronous sparse convolutional networks. In European Conference on Computer Vision. Springer, 415–431.
- [20] Shu Miao, Guang Chen, Xiangyu Ning, Yang Zi, Kejia Ren, Zhenshan Bing, and Alois Knoll. 2019. Neuromorphic vision datasets for pedestrian detection, action recognition, and fall detection. Frontiers in neurorobotics 13 (2019), 38.
- [21] Ivan V Oseledets. 2011. Tensor-train decomposition. SIAM Journal on Scientific Computing 33, 5 (2011), 2295–2317.
- [22] Christoph Posch, Teresa Serrano-Gotarredona, Bernabe Linares-Barranco, and Tobi Delbruck. 2014. Retinomorphic event-based vision sensors: bioinspired cameras with spiking output. Proc. IEEE 102, 10 (2014), 1470–1484.
- [23] Charles R Qi, Hao Su, Kaichun Mo, and Leonidas J Guibas. 2017. Pointnet: Deep learning on point sets for 3d classification and segmentation. In Proceedings of the IEEE conference on computer vision and pattern recognition. 652–660.
- [24] Charles Ruizhongtai Qi, Li Yi, Hao Su, and Leonidas J Guibas. 2017. Pointnet++: Deep hierarchical feature learning on point sets in a metric space. Advances in neural information processing systems 30 (2017).
- [25] Hongwei Ren, Chenghao Li, Xinyi Zhang, Chenchen Ding, Changhai Man, and Hao Yu. 2021. Atfvo: An attentive tensor-compressed Istm model with optical flow features for monocular visual odometry. In 2021 WRC Symposium on Advanced Robotics and Automation (WRC SARA). IEEE, 79–85.
- [26] Ali Samadzadeh, Fatemeh Sadat Tabatabaei Far, Ali Javadi, Ahmad Nickabadi, and Morteza Haghir Chehreghani. 2020. Convolutional spiking neural networks for spatio-temporal feature extraction. arXiv preprint arXiv:2003.12346 (2020).
- [27] Yusuke Sekikawa, Kosuke Hara, and Hideo Saito. 2019. Eventnet: Asynchronous recursive event processing. In Proceedings of the IEEE/CVF Conference on Computer Vision and Pattern Recognition. 3887–3896.
- [28] Du Tran, Lubomir Bourdev, Rob Fergus, Lorenzo Torresani, and Manohar Paluri. 2015. Learning spatiotemporal features with 3d convolutional networks. In Proceedings of the IEEE international conference on computer vision. 4489–4497.
- [29] Qinyi Wang, Yexin Zhang, Junsong Yuan, and Yilong Lu. 2019. Space-time event clouds for gesture recognition: From RGB cameras to event cameras. In 2019 IEEE Winter Conference on Applications of Computer Vision (WACV). IEEE, 1826–1835.
- [30] Qinyi Wang, Yexin Zhang, Junsong Yuan, and Yilong Lu. 2020. 'ST-EVNet: Hierarchical spatial and temporal feature learning on space-time event clouds. Proc. Adv. Neural Inf. Process. Syst. (NeurlIPS) (2020).
- [31] Wenxuan Wu, Zhongang Qi, and Li Fuxin. 2019. Pointconv: Deep convolutional networks on 3d point clouds. In Proceedings of the IEEE/CVF Conference on Computer Vision and Pattern Recognition. 9621–9630.
- [32] Bochen Xie, Yongjian Deng, Zhanpeng Shao, Hai Liu, and Youfu Li. 2022. VMV-GCN: Volumetric Multi-View Based Graph CNN for Event Stream Classification. IEEE Robotics and Automation Letters 7, 2 (2022), 1976–1983.
- [33] Jiancheng Yang, Qiang Zhang, Bingbing Ni, Linguo Li, Jinxian Liu, Mengdie Zhou, and Qi Tian. 2019. Modeling point clouds with self-attention and gumbel subset sampling. In Proceedings of the IEEE/CVF conference on computer vision and pattern recognition. 3323–3332.
- [34] Man Yao, Huanhuan Gao, Guangshe Zhao, Dingheng Wang, Yihan Lin, Zhaoxu Yang, and Guoqi Li. 2021. Temporal-wise attention spiking neural networks for event streams classification. In Proceedings of the IEEE/CVF International Conference on Computer Vision. 10221–10230.
- [35] Hengshuang Zhao, Li Jiang, Jiaya Jia, Philip HS Torr, and Vladlen Koltun. 2021. Point transformer. In Proceedings of the IEEE/CVF International Conference on Computer Vision. 16259–16268.